50806: amphibolite, Westonia

(Youanmi Terrane, Yilgarn Craton)

De Paoli, MC, Blereau, ER, Korhonen, FJ and Kelsey, DE

Location and sampling

Southern Cross (SH 50-16), Westonia (2635)

MGA Zone 50, 656701E 6539800N

WAROX site GSD050806

Sampled on 1 January 1976 (date entered)

This sample was collected from a low outcrop, about 14.3 km south of Wooded Hill, 4.1 km west-northwest of the Edna May Mine and 1.3 km north of Stoneman Road.

Geological context

The unit sampled is an amphibolite of the western Youanmi Terrane of the southwest Yilgarn Craton (Quentin de Gromard et al., 2021). This unit is part of a northwest-trending belt of Archean metasedimentary and gneissic rocks previously assigned to the South West Terrane and referred to informally by Wilde (2001) as the 'Lake Grace domain' (cf. Pidgeon et al., 2010). However, a recent reinterpretation places the boundary between the South West and the Youanmi Terranes farther to the southwest than shown on older maps (Quentin de Gromard et al., 2021). The Youanmi Terrane contains both granite–greenstone and high-grade gneiss components with emplacement ages from c. 3010 to 2600 Ma (Quentin de Gromard et al., 2021; Cassidy et al., 2006). Existing geochronological data from this part of the Youanmi Terrane is sparse. A metamonzogranite, collected about 43 km to the west-northwest of this locality, yielded an igneous crystallization age of 2662 ± 5 Ma (GSWA 224441, Wingate et al., 2021). A biotite metamonzogranite, collected about 45 km to the east of this locality, yielded an igneous crystallization age of 2639 ± 7 Ma (GSWA 182783, Wingate et al., 2015). The timing of high-grade metamorphism in the southwest Yilgarn is broadly constrained at 2665–2635 Ma (Korhonen et al., 2021).

Petrographic description

The sample is a strongly foliated, fine- to medium-grained amphibolite containing about 35% hornblende, 19% K-feldspar, 18% plagioclase, 11% biotite, 6% muscovite, 6% epidote, 1% clinopyroxene, 1% quartz, 1% chlorite, minor pyrrhotite and titanite, and trace amounts of pyrite, apatite and zircon (Fig. 1; Table 1). The sample has a granoblastic, polygonal to interlobate texture dominated by hornblende, K-feldspar, plagioclase and biotite, with subordinate epidote, clinopyroxene and quartz. Layers of K-feldspar–plagioclase and hornblende–biotite–clinopyroxene±epidote define a strong foliation (Fig. 1). Finer grained layers comprising saussuritized feldspar and/or intergrown albitic plagioclase–epidote (clinozoisite)±muscovite (sericite)±chlorite form predominately within the felsic domains (Fig. 2). Green-brown hornblende forms euhedral to subhedral grains up to 0.5 mm in diameter throughout the matrix and around clinopyroxene-rich domains (Fig. 2). Hornblende commonly contains inclusions of quartz, feldspar and biotite (Fig. 2b). Plagioclase is present as subhedral grains less than 1 mm in size that are closely associated with K-feldspar in the matrix and as subhedral to anhedral grains less than 200 µm in size commonly aligned with the foliation and along the margins of larger feldspar and biotite grains. Biotite occurs as elongate grains up to 1 mm in length. Muscovite occurs as very fine-grained sericite intergrown with feldspar, suggestive of recrystallization and pseudomorphic growth after primary feldspar. Very fine-grained, plumose intergrowths of epidote–clinozoisite and albitic plagioclase define aggregates that form shapes suggestive of pseudomorphs after feldspar. Epidote grains up to 350 µm in diameter occur in rare discontinuous layers aligned with the foliation (Fig. 2b). Clinopyroxene up to 1 mm in size is present in polymineralic aggregates that define local lenses and discontinuous layers (Fig. 1). These domains are

aligned with the foliation and also contain feldspar, quartz, epidote and titanite, rarely biotite, and are typically devoid of hornblende. Titanite is up to 350 µm in size and may either overgrow hornblende and biotite or may armour sulfide intergrowths and/or clinopyroxene. Rare grains of pyrrhotite and pyrite up to 250 µm in size occur throughout the matrix and are commonly closely associated with epidote or clinopyroxene. Rare zircon is up to 350 µm in size and occurs distributed throughout the sample.

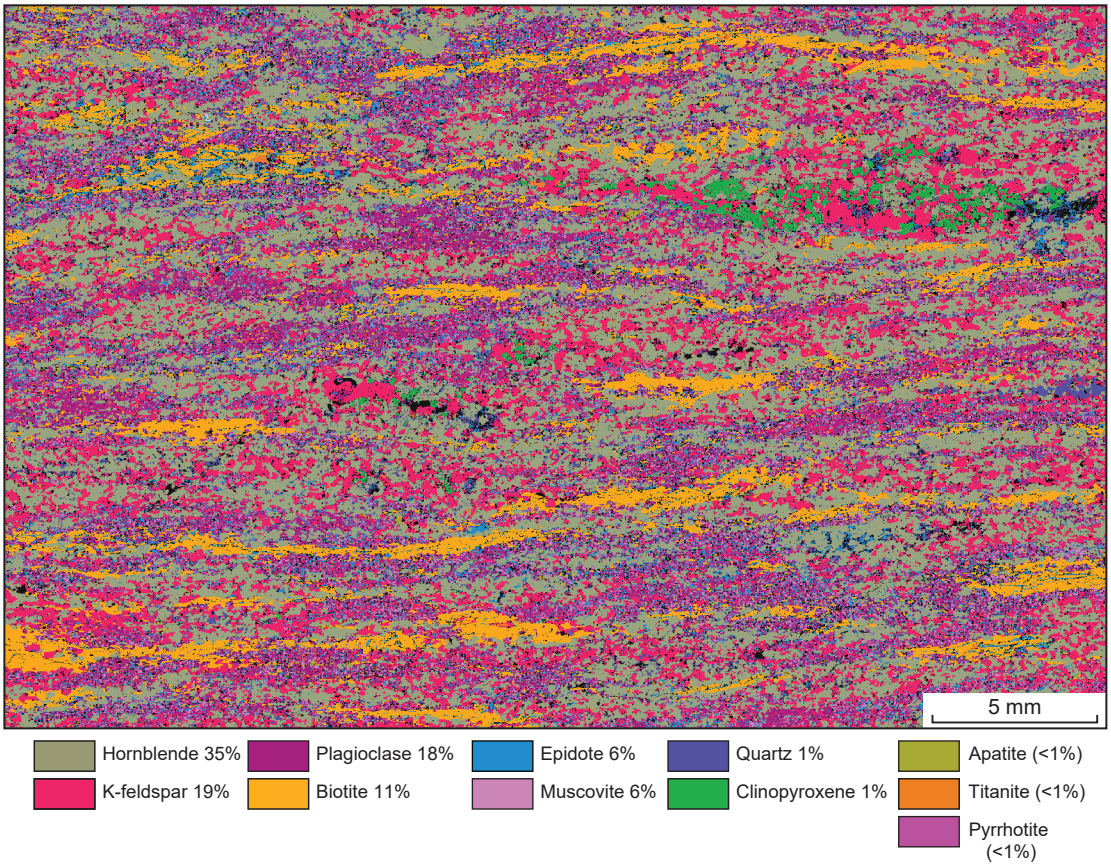

Figure 1. **TESCAN Integrated Mineral Analyser (TIMA) image of an entire thin section from sample 50806: amphibolite, Westonia. Volume percent proportions of major rock-forming minerals are calculated by the TIMA software. Black shows unclassified material**

Table 1. Mineral modes for sample 50806: amphibolite, Westonia

Mineral modes	Hbl	Kfs	Pl	Bt	Ms[b]	Qz	Cpx	Ep	Chl[b]	Ttn	Po	Py	H_2O	Liq
Observed (vol%)[a]	35	19	18	11	6	1	1	6	1	trace	trace	trace	–	–
Predicted (mol%)														
@ 3.3 kbar, 580 °C	14.7	12.6	24.5	28.6	–	9.8	9.0	–	–	0.8	–	–	–	–
@ 5.6 kbar, 665 °C	14.7	12.6	23.3	28.3	–	10.1	10.5	–	–	0.5	–	–	0.1	–
@ 5 kbar, 680 °C	9.3	10.7	25.1	31.1	–	10.1	12.4	–	–	0.2	–	–	–	1.0
@ 8 kbar, 715 °C	24.1	14.7	18.3	22.8	–	9.6	9.3	–	–	0.2	–	–	–	1.1
@ 9 kbar, 749 °C	28.3	15.6	15.9	19.9	–	9.2	9.3	–	–	0.0	–	–	–	1.9

NOTES: (a) Minor titanite, pyrrhotite, pyrite, and chlorite, and trace zircon also present in thin section
(b) Intepreted as retrograde
– not present

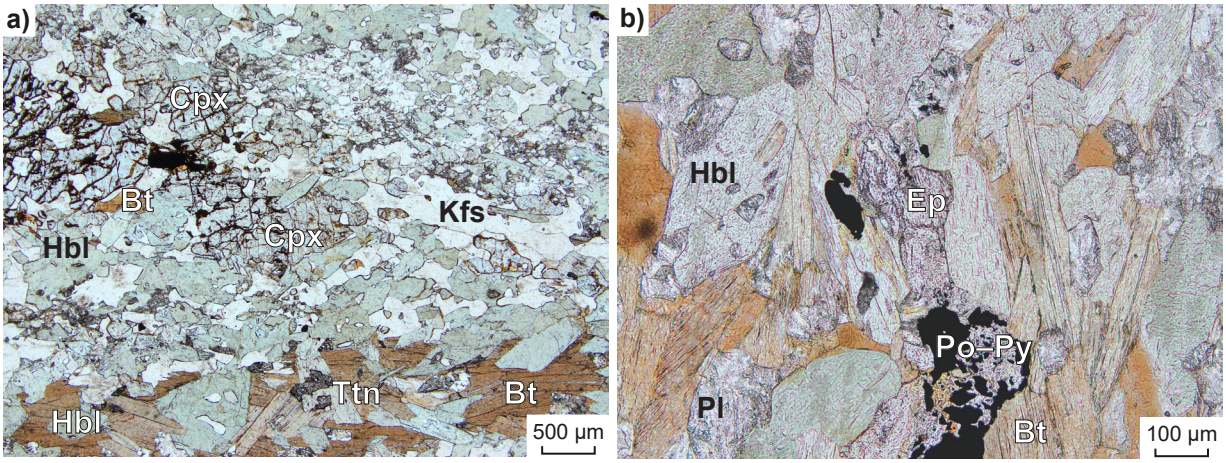

Figure 2. **Photomicrographs in plane-polarized light of sample 50806: amphibolite, Westonia. Abbreviations: Bt, biotite; Cpx, clinopyroxene; Ep, epidote; Hbl, hornblende; Kfs, K-feldspar; Pl, plagioclase; Po, pyrrhotite; Py, pyrite; Ttn, titanite**

Analytical details

The metamorphic evolution of this sample was investigated using phase equilibria modelling, based on the bulk-rock composition (Table 2). The composition was determined by X-ray fluorescence spectroscopy, together with loss on ignition (LOI). FeO content was analysed by Fe^{2+} titration (as 85% of total Fe), and Fe_2O_3 calculated by difference. The modelled O content (for Fe^{3+}) was increased (to 30% of total Fe as Fe^{3+}) from the titration value (= 15%) on the basis of T–M_O modelling (not shown; see Korhonen et al., 2020 for details) as preliminary investigations using the titrated value did not stabilize hornblende. H_2O content equal to the measured LOI (= 2.6 mol%) also did not allow for the stability of the observed mineral assemblage. Therefore, an appropriate H_2O content was evaluated using a T–M_{H2O} pseudosection (not shown). The modelled H_2O content (= 4.3 mol%; Table 2) was required to be higher than LOI in order to reproduce the peak assemblage at the lowest H_2O contents; higher H_2O contents do not significantly change the topology close to the solidus but do increase the calculated mode of melt. The bulk composition was also adjusted for the presence of apatite by applying a correction to calcium and for pyrite by applying a correction to iron (Table 2).

Thermodynamic calculations were performed in the NCKFMASHTO (Na_2O–CaO–K_2O–FeO–MgO–Al_2O_3–SiO_2–H_2O–TiO_2–O) system using THERMOCALC version tc340 (Powell and Holland, 1988; updated October 2013) and the internally consistent thermodynamic dataset of Green et al. (2016; version dataset tc-ds62, created January 2015). The activity–composition relations used in the modelling are detailed in Green et al. (2016); the augite model was used for clinopyroxene. Additional information on the workflow with relevant background and methodology are provided in Korhonen et al. (2020).

Table 2. Measured whole-rock and modelled compositions for sample 50806: amphibolite, Westonia

XRF whole-rock composition (wt%)[a]

SiO_2	TiO_2	Al_2O_3	Fe_2O_3[b]	FeO[b]	MnO	MgO	CaO	Na_2O	K_2O	P_2O_5	LOI	Total
49.42	0.88	16.73	1.43	7.08	0.15	7.10	8.50	0.80	4.91	0.10	1.85	98.95

Normalized composition used for phase equilibria modelling (mol%)

SiO_2	TiO_2	Al_2O_3	O[c]	FeO^T[d]	MnO	MgO	CaO[e]	Na_2O	K_2O	–	H_2O[f]	Total
51.78	0.69	10.33	1.08	7.09	–	11.09	9.40	0.81	3.28	–	4.45	100

NOTES:
(a) Data and analytical details are available from the WACHEM database <www.dmirs.wa.gov.au/launch/geochemistry>
(b) FeO analysed by Fe^{2+} titration; Fe_2O_3 content calculated by difference
(c) O content (for Fe^{3+}) based on titration value
(d) FeO^T = moles FeO + 2 * moles O. Modified to remove pyrite = moles FeO^T - 0.5 * (moles SO_2), where SO_2 moles = 0.455
(e) CaO modified to remove apatite: CaO(Mod) = CaO(Total) - (moles CaO(in Ap) = 3.33 * moles P_2O_5)
(f) H_2O content based on T–M_{H2O} diagram; see text for additional details

Results

Metamorphic *P–T* estimates have been derived based on detailed examination of one thin section and the bulk-rock composition; care was taken to ensure that the thin section and the sample volume selected for whole-rock chemistry were similar in terms of featuring the same minerals in approximately the same abundances (Table 1), to minimize any potential compositional differences. The *P–T* pseudosection was calculated over a *P–T* range of 2–12 kbar and 500–800 °C (Fig. 3). The solidus is located between 665 and 795 °C across the range of modelled pressures. K-feldspar, biotite and quartz are stable across the range of modelled pressure and temperature. Plagioclase is stable over the modelled temperature range, although it becomes increasingly less stable at high pressure (>7 kbar). Clinopyroxene is stable over the entire modelled *P–T* range except for very high temperatures and pressures. Garnet is stable at high pressure, with a minimum stability of 6 kbar at 500 °C. Amphibole (hornblende) is stable over much of the modelled *P–T* range, except at low *P*–high *T* (<4.5 kbar, >595 °C). Epidote is stabilized at increasingly high pressures and temperatures, above 2 kbar at 505 °C and above 11.1 kbar at 800 °C. Titanite is stable above 2 kbar at 630 °C through to 10.8 kbar at 800 °C, and is replaced by rutile to higher pressures (>8.1 kbar at 500 °C) and by ilmenite at high *T*–low *P*. The equilibria is H_2O-saturated in a triangular region immediately below the solidus, with a maximum stability of 6 kbar between 575 and 695 °C.

Interpretation

Based on the coarse grain size, polygonal texture and mineral associations that support textural equilibrium, the peak metamorphic assemblage is interpreted to contain hornblende, clinopyroxene, plagioclase, K-feldspar, biotite, titanite and quartz. Distinct, localized clinopyroxene-rich domains, also containing feldspar, quartz, minor titanite, pyrrhotite–pyrite, epidote and rare biotite, commonly form lenses that are mantled by hornblende. These domains could represent leucocome, suggesting that a small volume of melt may have been part of the peak assemblage. The relationship of epidote with the peak minerals is ambiguous. Fine-grained, disseminated epidote–clinozoisite that occurs within intergrowths of albitic plagioclase and/or with sericite is interpreted to be a retrograde pseudomorph after feldspar. These grains are texturally distinct from the coarser grained epidote aligned in the matrix (Fig. 2b). Pyrrhotite–pyrite also occur as rare grains with the coarser grained epidote in the matrix, but the relative timing with the epidote is also unclear. It is possible that coarser grained epidote was part of the peak assemblage, but it could also be interpreted as a fluid induced, post-peak mineral.

If melt was stable at the peak of metamorphism, the peak assemblage of hornblende–clinopyroxene–plagioclase–K-feldspar–biotite–titanite–quartz–melt is stable between 665 and 770 °C at 4.6 – 10.0 kbar. However, the former presence of both melt and H_2O cannot be unequivocally verified. Given these uncertainties, the peak assemblage could also be hornblende–clinopyroxene–plagioclase–K-feldspar–biotite–titanite–quartz–H_2O, with a *P–T* stability of 2.6 – 5.9 kbar and 590–675 °C, or hornblende–clinopyroxene–plagioclase–K-feldspar–biotite–titanite–quartz, with a *P–T* stability of 2.6 – 3.6 kbar and 540–600 °C. The peak fields are delimited by the loss of titanite and the stability of ilmenite at higher temperature, the stability of epidote and Fe–Ti oxides at lower temperature, the loss of hornblende at lower pressure, and the stability of epidote and garnet at higher pressure. There are some differences between the predicted mineral modes over the peak fields with the modes observed in thin section (Table 1). These discrepancies may be accounted for by a number of factors, including: 1) the growth of new retrograde phases, such as muscovite (sericite), titanite, epidote–clinozoisite and albitic plagioclase; 2) the growth or consumption of peak phases during retrogression; 3) the potential issues arising from the use of the activity–composition models for hornblende and clinopyroxene that have compounded effects on the stability of other phases such as biotite (e.g. Forshaw et al., 2019).

Some fine-gained epidote–clinozoisite, titanite, muscovite (sericite), and potentially pyrrhotite–pyrite intergrowths are interpreted to be recrystallized post-peak minerals, possibly fluid induced. The fine-grained, variable distribution of sulfide may also suggest that it formed part of the original peak assemblage and was subsequently partially retrogressed. Recrystallization of feldspar and the formation of post-peak epidote–clinozoisite and titanite could grow along a retrograde path with a decrease in temperature, with or without a decrease in pressure.

Peak metamorphic conditions are estimated at 540–770 °C and 2.6 – 10 kbar. However, the possibility of low volume partial melting would refine conditions to 665–770 °C and 4.6 – 10 kbar, with an apparent thermal gradient between 75 and 120 °C/kbar. There is no information on the prograde evolution, and little definitive information on the retrograde path; therefore the overall shape of the *P–T* path is not defined.

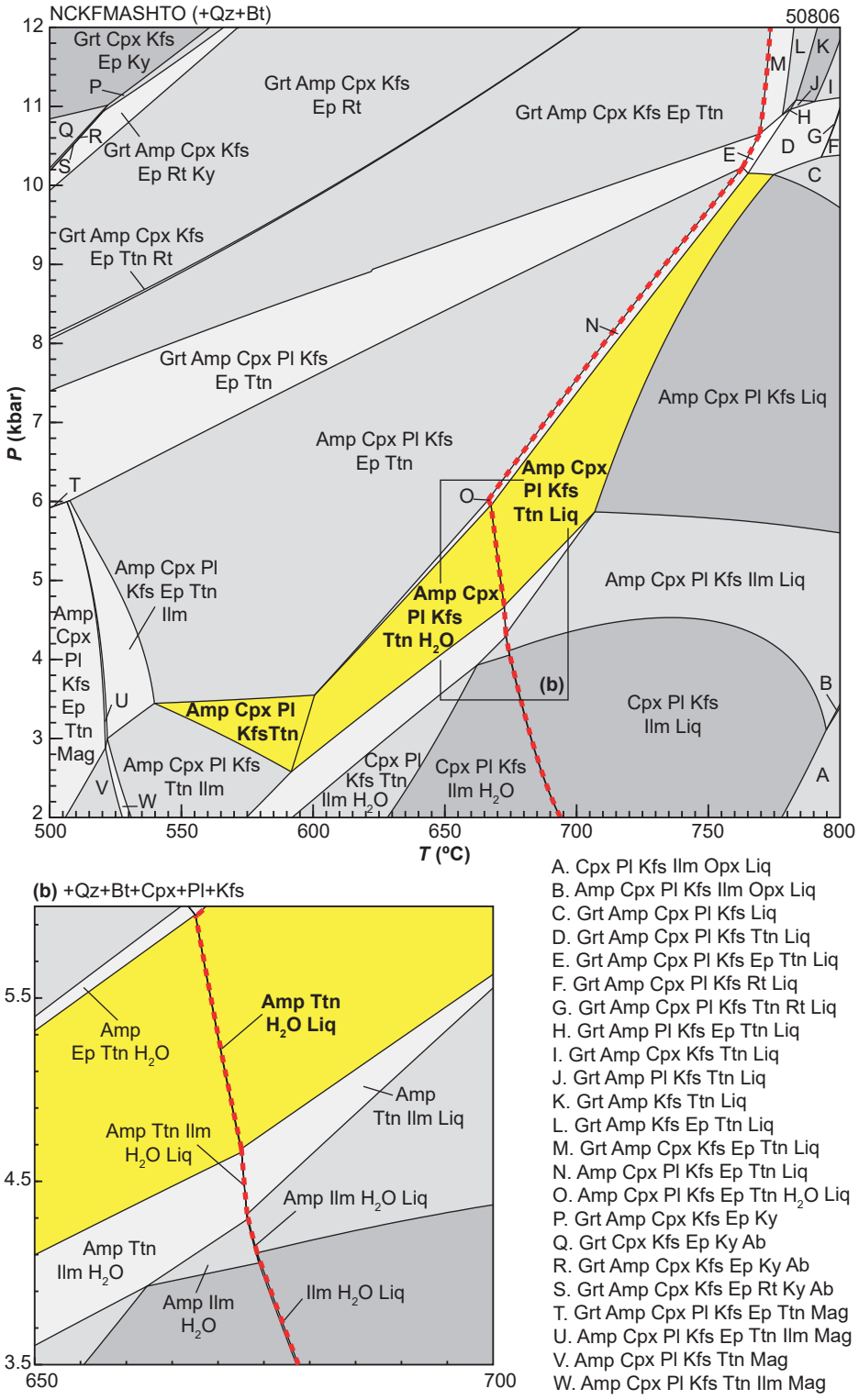

Figure 3. ***P–T*** **pseudosection calculated for sample 50806: amphibolite, Westonia. Assemblage fields corresponding to peak metamorphic conditions is shown in bold text and yellow shading. Red dashed line represents the solidus. Abbreviations: Ab, albite; Amp, amphibole (hornblende); Bt, biotite; Cpx, clinopyroxene; Ep, epidote; Grt, garnet; H_2O, fluid (pure H_2O); Ilm, Ilmenite; Kfs, K-feldspar; Ky, kyanite; Liq, silicate melt; Mag, magnetite; Opx, orthopyroxene; Pl, plagioclase; Qz, quartz; Rt, rutile; Ttn, titanite**

References

Cassidy, KF, Champion, DC, Krapež, B, Barley, ME, Brown, SJA, Blewett, RS, Groenewald, PB and Tyler, IM 2006, A revised geological framework for the Yilgarn Craton, Western Australia: Geological Survey of Western Australia, Record 2006/8, 8p.

Forshaw, JB, Waters, DJ, Pattison, DRM, Palin, RM and Gopon, P 2019, A comparison of observed and thermodynamically predicted phase equilibria and mineral compositions in mafic granulites: Journal of Metamorphic Geology, v. 37, p. 153–179.

Green, ECR, White, RW, Diener, JFA, Powell, R, Holland, TJB and Palin, RM 2016, Activity-composition relations for the calculation of partial melting equilibria in metabasic rocks: Journal of Metamorphic Geology, v. 34, no. 9, p. 845–869.

Korhonen, FJ, Blereau, ER, Kelsey, DE, Fielding, IOH and Romano, SS 2021, Metamorphic evolution of the southwest Yilgarn, *in* Accelerated Geoscience Program extended abstracts: Geological Survey of Western Australia Record 2021/4, p. 108–115.

Korhonen, FJ, Kelsey, DE, Fielding IOH and Romano, SS 2020, The utility of the metamorphic rock record: constraining the pressure–temperature–time conditions of metamorphism: Geological Survey of Western Australia, Record 2020/14, 24p.

Quentin de Gromard, R, Ivanic, TJ and Zibra, I 2021, Pre-Mesozoic interpreted bedrock geology of the southwest Yilgarn, 2021, *in* Accelerated Geoscience Program extended abstracts: Geological Survey of Western Australia, Record 2021/4, p. 122–144.

Pidgeon, RT, Wingate, MTD, Bodorkos, S and Nelson, DR 2010, The age distribution of detrital zircons in quartzites from the Toodyay – Lake Grace Domain, Western Australia: implications for the early evolution of the Yilgarn Craton: American Journal of Science, v. 310, p. 1115–1135.

Powell, R and Holland, TJB 1988, An internally consistent dataset with uncertainties and correlations: 3. Applications to geobarometry, worked examples and a computer program: Journal of Metamorphic Geology, v. 6, no. 2, p. 173–204.

Wilde, SA 2001, Jimperding and Chittering metamorphic belts, Western Australia— a field guide: Geological Survey of Western Australia, Record 2001/12, 24p.

Wingate, MTD, Kirkland, CL and Doublier, MP 2015, 182783: biotite metamonzogranite, Nurdungarra Rock; Geochronology Record 1248: Geological Survey of Western Australia, 3p.

Wingate, MTD, Lu, Y, Fielding, IOH and Smithies, RH 2021, 224441: metamonzogranite, Knungajin Hill; Geochronology Record 1789: Geological Survey of Western Australia, 4p.

Links

Record 2020/14 The utility of the metamorphic rock record: constraining the pressure–temperature–time conditions of metamorphism

Recommended reference for this publication

De Paoli, MC, Blereau, ER, Korhonen, FJ and Kelsey, DE 2022, 50806: amphibolite, Westonia; Metamorphic History Record 26: Geological Survey of Western Australia, 7p.

Data obtained: 22 August 2022

Date released: 7 October 2022

This Metamorphic History Record was last modified on 5 October 2022

Grid references in this publication refer to the Geocentric Datum of Australia 1994 (GDA94). All locations are quoted to at least the nearest 100 m.

WAROX is GSWA's field observation and sample database. WAROX site IDs have the format 'ABCXXXnnnnnnSS', where ABC = geologist username, XXX = project or map code, nnnnnn = 6 digit site number, and SS = optional alphabetic suffix (maximum 2 characters).

Isotope and element analyses are routinely conducted using the GeoHistory laser ablation ICP-MS and Sensitive High-Resolution Ion Microprobe (SHRIMP) ion microprobe facilities at the John de Laeter Centre (JdLC), Curtin University, with the financial support of the Australian Research Council and AuScope National Collaborative Research Infrastructure Strategy (NCRIS). The TESCAN Integrated Mineral Analyser (TIMA) instrument was funded by a grant from the Australian Research Council (LE140100150) and is operated by the JdLC with the support of the Geological Survey of Western Australia, The University of Western Australia (UWA) and Murdoch University. Mineral analyses are routinely obtained using the electron probe microanalyser (EPMA) facilities at the Centre for Microscopy, Characterisation and Analysis, UWA, at Adelaide Microscopy, University of Adelaide, and at the Electron Microscopy and X-ray Microanalysis Facility, University of Tasmania.

Digital data related to WA Geology Online, including geochronology and digital geology, are available online at the Department's Data and Software Centre and may be viewed in map context at GeoVIEW.WA.

Further details of geoscience products are available from:
Information Centre
Department of Mines, Industry Regulation and Safety
100 Plain Street
EAST PERTH WA 6004
Telephone: +61 8 9222 3459 | Email: publications@dmirs.wa.gov.au
www.dmirs.wa.gov.au/GSWApublications